Effects of Size on the Dynamics of Dislocations in Ice Single Crystals

V. Taupin,[1] S. Varadhan,[2] J. Chevy,[3] C. Fressengeas,[1] A. J. Beaudoin,[2] M. Montagnat,[3] and P. Duval[3]

[1]*Laboratoire de Physique et Mécanique des Matériaux, Université Paul Verlaine-Metz/CNRS, Ile du Saulcy, 57045 Metz Cedex, France*

[2]*Department of Mechanical Sciences and Engineering, University of Illinois at Urbana-Champaign, 1206 West Green Street, Urbana, Illinois 61801, USA*

[3]*Laboratoire de Glaciologie et Géophysique de l'Environnement–CNRS, 54 rue Molière, 38402 Saint Martin d'Hères Cedex, France*

(Received 5 March 2007; published 12 October 2007)

Single crystals of ice subjected to primary creep in torsion exhibit a softening behavior: the plastic strain rate increases with time. In a cylindrical sample, the size of the radius affects this response. The smaller the radius of the sample becomes while keeping constant the average shear stress across a section, the softer the response. The size-dependent behavior is interpreted by using a field dislocation theory, in terms of the coupled dynamics of excess screw dislocations gliding in basal planes and statistical dislocations developed through cross slip occurring in prismatic planes. The differences in the results caused by sample height effects and variations in the initial dislocation microstructure are discussed.

DOI: 10.1103/PhysRevLett.99.155507 PACS numbers: 61.72.Lk, 62.20.Fe, 81.40.Lm, 83.80.Nb

In a torsion test, shear stress increases from the axis to the exterior of the sample. When investigating the plastic response of materials, this gradient is commonly viewed as a drawback of torsion testing. It becomes beneficial when the material behavior involves internal length scales associated with emerging dislocation structures. The inhomogeneity of the boundary conditions then generates ''excess dislocations,'' which give rise to long-range elastic stress fields. As an hcp material with a strong anisotropy, ice is a choice material in this respect. It deforms plastically by the activity of basal slip systems almost exclusively [1] and it is characterized by a low Peierls stress [2]. Anisotropy and a low lattice friction favor long-range elastic interactions and dislocation transport, as well as their interactions. Indeed, as will be shown in this Letter, the creep response of ice single crystals oriented for basal slip in torsion exhibits size effects in the cm range. Hence, this problem is in turn a challenging case for theories of plasticity with internal length scales. The torsion of thin copper wires with diameters in the range 12–170 μm has been used in order to probe into such theories [3], but the large strains achieved, the polycrystalline character of the material, the texture evolution, and varying grain size of the samples may have complicated the interpretation. The purpose of the present work is to describe the creep response of ice single crystals in torsion, a much simpler material and experimental configuration, with emphasis on the effects of the sample dimensions on this response. Original experimental data are presented and an interpretation for the observed behavior is proposed within the framework of a nonlocal field theory for the dynamics of excess and statistical dislocations [4,5]. In this theory, excess dislocation densities are regarded as being a continuous manifestation of lattice incompatibility. They are nonuniformly distributed and associated with the development of long-range lattice curvature and internal stress fields. In contrast, statistical dislocations can be uniformly distributed. They contribute to statistical hardening through short-range interactions, but not to internal stresses buildup. In conventional (local) plasticity theories, only statistical dislocations are considered. Both species contribute to plastic flow, however. Their dynamics are coupled, for spatial gradients in the plastic deformation due to statistical dislocations generate excess dislocations. The present theory draws on seminal work by Kröner [6] and Mura [7]. Approaches similar in spirit include those in Refs. [8–12].

Laboratory grown single crystals were used for the torsion experiments. All samples were machined from these crystals in the form of cylinders, with radius R in the range 13–24 mm. The samples height h was kept in the range 57–60 mm. The grips were conveniently made from water refrozen at the interface sample machine, and the temperature was maintained at $-11 \pm 1\,^{\circ}\mathrm{C}$. A constant positive torque M was applied to the sample. The average shear stress across a sample section $\bar{\tau} = 3M/2\pi R^3$ was maintained of the order of 0.1 MPa. When torsion is uniform along the axis, the shear strain γ at radius r is $\gamma = \kappa r$, where $\kappa = \theta/h$ is the constant twist per unit length of the sample. Possible deviations from macroscopic uniformity were checked by monitoring lines drawn on the outer surface, parallel to the axis. The data were discarded when significant deviations occur. Figure 1 shows creep curves, i.e., plots of $\Gamma = \kappa R$, the strain on the outer surface, vs time. Straining of the samples was interrupted at $\Gamma = 4.5\%$, a value of strain still in the range of primary transient creep. The maximum twist was then $\theta \approx 0.2$ rad. From dimensional analysis it is seen that, for a material devoid of internal length scales, creep curves gathered from samples with varying radius superpose if the average shear stress $\bar{\tau}$ is kept constant. Conversely, distinct curves in this plot are evidence for an effect of size on the plastic response. Figure 1 suggests that the time needed to achieve a given strain decreases when the radius is reduced under constant average shear stress, which indicates a softening

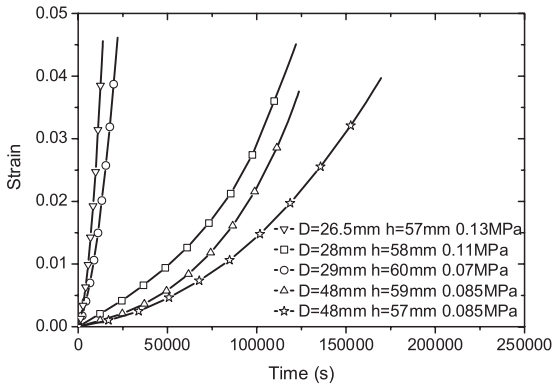

FIG. 1. Creep strain on outer surface vs time, for various diameter D values. Height and average shear stress are indicated.

effect of radius reduction on the sample response. Dispersion in the curves exists, but is limited. It results mainly from uncontrollable fluctuations in the initial dislocation microstructure, which lead to uneven initial creep strain rates. End effects due to the small variation in the sample height were checked to be very limited.

Interpretation in terms of dislocation dynamics of these observations will be given on the basis of the model described below. It should be noticed at once that x-ray diffraction analyses performed on samples extracted from the strained cylinders show that plasticity of the samples is almost exclusively due to excess dislocations of screw character gliding in basal planes, with very few mobile statistical dislocations [13]. The initial density of dislocations present in the samples, mostly sessile dislocations, is shown to be less than 10^8 m^{-2}. In addition, the analyses reveal a scale invariant arrangement of excess dislocations along the torsion axis. The latter can be explained by the occurrence of double cross-slip of screw dislocations through prismatic planes [14]. Diffusion-controlled climb of dislocation on planes normal to the basal planes should be very limited due to the low value of diffusion coefficients in ice. Formally, however, cross-slip and climb are treated in the same way as out-of-plane motion of dislocations in the forthcoming model.

The model uses the continuum description of dislocations based upon Nye's dislocation density tensor α [15]. Operating on the normal $\mathbf{n}$ to a unit surface S, α provides the net Burgers vector $\mathbf{b} = \alpha.\mathbf{n}$ of all dislocations lines threading S, i.e., the incompatibility in displacement found along the Burgers circuit surrounding this surface. Because of this incompatibility, the elastic distortion tensor $\mathbf{U_e}$ is not a gradient. It has an incompatible part, $\mathbf{U_e}^{\perp}$, which results from the distribution α and is a solution to the incompatibility equation

$$\mathbf{curl}\mathbf{U}_{\mathbf{e}}^{\perp} = \alpha, \tag{1}$$

written here at small strains. Its compatible part, $\mathbf{U}_{\mathbf{e}}^{\parallel}$, is a gradient. For small strains, it is the difference between the displacement gradient $\mathbf{U} = \mathbf{grad}\ \mathbf{u}$ and the compatible part of the plastic distortion, $\mathbf{U}_{\mathbf{p}}^{\parallel}$. At the resolution scale used in the present problem (the characteristic size of unit surface S), the total plastic distortion rate $\dot{\mathbf{U}}_{\mathbf{p}}$ results from the motion of the excess dislocations α, with (averaged over S) velocity $\mathbf{V}$, and of the statistical (mobile) dislocations through the conventional plastic velocity gradient tensor $\mathbf{L_p}$ (throughout the Letter, a superposed dot indicates a time derivative)

$$\dot{\mathbf{U}}_{\mathbf{p}} = \alpha \times \mathbf{V} + \mathbf{L_p}. \tag{2}$$

The incompatible part of $\dot{\mathbf{U}}_{\mathbf{p}}$ feeds the increment of excess dislocations through the transport equation for dislocation densities

$$\dot{\alpha} = -\mathbf{curl}\dot{\mathbf{U}}_{\mathbf{p}}. \tag{3}$$

The stress tensor $\mathbf{T}$ is obtained from the tensor of elastic constants $\mathbf{C_e}$ as

$$\begin{aligned}\mathbf{T} &= \mathbf{C_e}\colon \{\mathbf{U_e}\} = \mathbf{C_e}\colon \{\mathbf{U}_{\mathbf{e}}^{\parallel} + \mathbf{U}_{\mathbf{e}}^{\perp}\} \\ &= \mathbf{C_e}\colon \{\mathbf{grad}\,\mathbf{u} - \mathbf{U}_{\mathbf{p}}^{\parallel} + \mathbf{U}_{\mathbf{e}}^{\perp}\},\end{aligned} \tag{4}$$

where $\{\mathbf{A}\}$ denotes the symmetric part of tensor $\mathbf{A}$. It satisfies the equilibrium equation

$$\mathbf{div}\,\mathbf{T} = \mathbf{0}. \tag{5}$$

Complemented with constitutive relations for the dislocation velocity $\mathbf{V}$ as a function of stress and dislocation orientation, and for the evolution of the statistical densities involved in the velocity gradient $\mathbf{L_p}$, (1)–(5) form a complete set of equations, of hyperbolic character, for the evolution of stress and dislocation densities. Boundary conditions comprise the conventional stress and displacement conditions, and the specification of inward fluxes of dislocations. A more detailed account of this overarching framework can be found in [4,5].

Two types of solutions of Eqs. (1)–(5) are offered in what follows. First we provide a full 3D numerical solution by using a Galerkin—least squares finite element method appropriate for hyperbolic problems (see [5,16] for details). These detailed simulations provide for the identification of the mesoscale features at the origin of creep acceleration. A 1D model is then applied for a twofold purpose: to illustrate the critical aspects of the theory; to allow for effective parametric study of size effects. In this idealization for deformation under a gradient of simple shear, we consider circumferential screw dislocation density of infinite extent in the (x, z) directions, line and Burgers vector along x, and transport in y. The distributions of shear stress σ_{xz}, excess screw density α_{xx}, and mobile statistical density ρ_m along a sample radius are the unknowns. The resulting equations, derived from the complete set (1)–(5) in creep reduce to

$$\sigma_{xz,x} = \sigma_{xz,z} = 0, \tag{6}$$

$$\dot{\alpha}_{xx} + (\alpha_{xx} v_y)_{,y} = -(\rho_m b v)_{,y}. \tag{7}$$

Here b is the length of the Burgers vector, and a comma

TABLE I. Numerical constants used in the model.

b	v_0	σ_0	n	μ	β
4.5×10^{-10} m	3.6×10^{-7} m/s	0.1 MPa	2	3 GPa	0.1
$\bar{\alpha}$	$\tilde{\alpha}$	$\hat{\alpha}$	C_1	C_2	
0.133	0.666×10^{-2}	10^5	10^{-8}	17	

indicates a partial derivative. The shear stress σ_{xz} cannot be obtained from these simplified equations, and recourse is made to approximations. Since the concern is on transient primary creep and the sample remains mostly elastic in its central part, as will be discussed below, an elastic approximation is used: $\sigma_{xz} = (y/R)\tau$. It was checked that it differs from the stress distribution expected for a fully viscoplastic response by less than 15%. Equation (7) is a transport equation. Here it represents the transport of screw dislocations with a source term due to gradients in statistical dislocation mobility. Account of the physics of dislocation velocity and of straining history is now made through phenomenological statements. Following [1], we assume a power law relationship for the average excess and statistical dislocation velocities (v_y, v) in the form

$$v_y = v = v_0 \mathrm{sgn}(\sigma_{xz} - \sigma_\mu) \left(\frac{|\sigma_{xz} - \sigma_\mu|}{\sigma_0 + \sigma_h} \right)^n \tag{8}$$

with $n = 2$. Parameters (v_0, σ_0) are reference velocity and stress values, respectively. They are identified from the experimental data [1,2]. An isotropic statistical hardening is derived from the sessile density ρ_s in the Bailey-Hirsch form: $\sigma_h = \bar{\alpha}\mu b\sqrt{\rho_s}$, where μ denotes the elastic shear modulus and $\bar{\alpha}$ is a constant. Only a fraction $(1 - \beta)$ of the nucleated screws glides in the basal planes. They induce a backstress, with rate of formation

$$\dot{\sigma}_\mu = \tilde{\alpha}\mu\alpha_{xx}v_y - \frac{|v_y|}{\hat{\alpha}b}\sigma_\mu, \tag{9}$$

where ($\tilde{\alpha}$, $\hat{\alpha}$) are constants. Relation (9) is similar to the Armstrong-Frederick law for kinematic hardening [17], but here the backstress builds up from excess dislocation mobility only. Note that the involved relaxation time $\tau_r = \hat{\alpha}b/|v_y|$ is inversely proportional to the excess dislocation velocity. The complementary fraction β of nucleated excess screws experiences out-of-plane motion induced by the internal stress field. Therefore the statistical sessile density increases—due to the formation of edge segments in prismatic planes, assumed to be proportional to the rate of screw nucleation

$$\dot{\rho}_s = \frac{\beta}{b}|\dot{\alpha}_{xx}|. \tag{10}$$

In our calculations, σ_h remains smaller than the reference stress σ_0, implying that statistical hardening is relatively insignificant, whereas the backstress σ_μ can be of the order of the applied stress τ. The statistical mobile dislocation density ρ_m has a very low initial value. It increases due to dislocation sources associated with edge jogs in prismatic planes [18]. Its nucleation rate is supposed to be proportional to the shear strain rate, with coefficient C_1. Saturation of mobile dislocations results from their mutual annihilation, with coefficient C_2.

TABLE II. Initial conditions.

ρ_m	ρ_s	$\alpha_{xx}(R)$
10^6 m^{-2}	10^8 m^{-2}	0.32 m^{-1}

$$\dot{\rho}_m = \left(\frac{C_1}{b^2} - C_2\rho_m \right) |\alpha_{xx}v_y + \rho_m b v|. \tag{11}$$

Parameters and initial conditions for the 1D model are given in Tables I and II, respectively. They are very similar in the 3D calculations. Initial conditions on screw dislocation density should be consistent with the observed initial strain rate $\dot{\Gamma}$. They should also enable us to reproduce the dislocation source distribution, mostly clustered along the sample edge. In this aim, we use a linear increase of the screw density from axis to edge, which leads to a parabolic source distribution. Note that out-of-plane dislocation motion and backstress buildup are automatically present in the 3D computations. Their presence in the 1D model is a phenomenological offset for the assumed invariance in the c-axis direction. Under a positive torque, an outstanding feature of both models is the nucleation of positive screw dislocations close to the sample edge, their transport towards the axis and, as stress and velocity decrease in this area, the formation of pileups. Figure 2 shows the (locally resolved) excess screw density and the shear component of the stress obtained from the 3D model. The excess screw density includes the development of a radial component [19] as a consequence of transport. Note that the 3D stress distribution supports the assumption made in the 1D idealization. As seen in Fig. 3, the continuous increase in the creep rate is retrieved from both models. The reverse torsion behavior, not discussed in this Letter for lack of space, is also fully retrieved. The excellent agreement suggests that nucleation and transport of the excess density

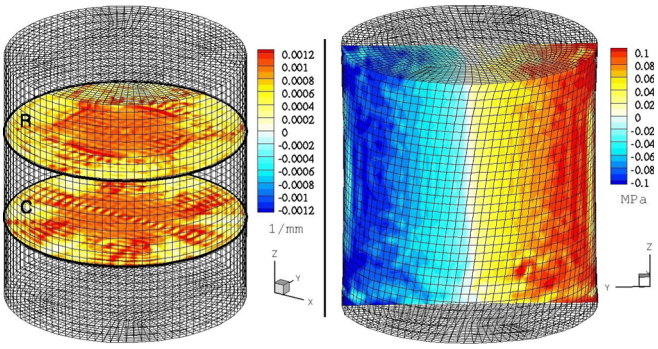

FIG. 2 (color online). Shown on left is the excess screw density on the undeformed mesh, locally resolved to indicate radial (R) and circumferential (C) components. At right, the shear stress component σ_{xz} is shown on the deformed mesh, with displacements scaled by a factor of 5.

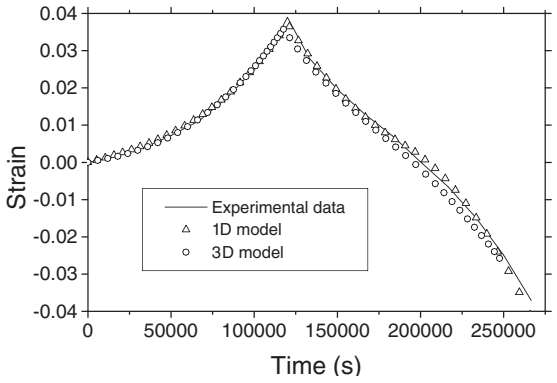

FIG. 3. Creep curves in forward and reverse torsion from experiments, 1D and 3D models.

are key aspects of the physical response. Further, when the gradient in stress is increased by downsizing the sample radius, screw nucleation is promoted and acceleration in the creep rate follows, in close agreement with experimental data (see Fig. 4). Thus, larger screw densities due to radius reduction do not imply hardening of the response, as would have been expected had these dislocations contributed to hardening like statistical dislocations. Rather, they induce softening due to larger rates of plastic distortion.

Size effects were evidenced in the creep response of ice single crystals in torsion. Under constant average shear stress, all other parameters being kept equal (or at least similar when their control is hardly possible, as in the case of the initial dislocation microstructure), reducing the radius of the sample leads to softening of the response, due to higher gradients. This trend is well reproduced by the model presented in the Letter. Basically, it is attributed to changes in excess screw dislocation nucleation: smaller radii promote screw nucleation, which in turn favors plastic distortion and response softening. In addition, the model asserts the role of long-range internal stresses in inducing the out-of-basal-plane dislocation motion responsible for the observed scale invariant dislocation structure (see [14]). It suggests that the edge jogs formed in prismatic planes in this process have a dual role, as they also act as obstacles to the basal glide of excess screw dislocations. In

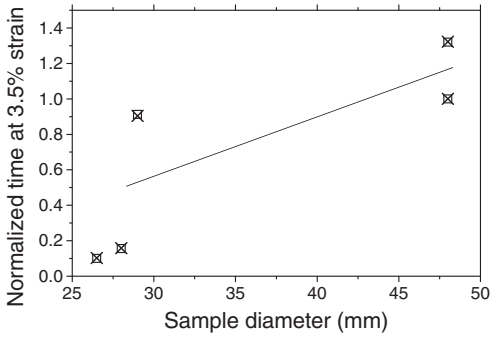

FIG. 4. Normalized time at 3.5% strain, experiments and modeling. Experimental data from creep tests shown in Fig. 1. The straight line suggests the trend.

velocity driven torsion testing of metals, evidence seems to be pointing at response hardening when the sample radius is reduced [3]. We note that observations similar in spirit to ours were made in order to interpret this ''anomalous'' hardening in copper [19,20]. In these references, the reduction in the density of excess screw dislocations in the center region of the sample is seen as the origin of hardening. As its plastic distortion is reduced, the metal behaves more like an elastic solid and becomes harder in this area. On the basis of our simulations, we believe that dislocation transport and backstress buildup are the controlling mechanisms for the rarefaction of excess screw dislocations in the center of the sample, through excess screw pileup formation.

A. B. and S. V. received support under U.S. Department of Energy Grant No. DEFG03-02-NA00072 and the Center for Simulation of Advanced Rockets at the University of Illinois at Urbana-Champaign (UIUC), U.S. DOE subcontract No. B341494. A. B., C. F., S. V., and V. T. benefited from exchanges under a joint agreement between Centre National de la Recherche Scientifique and UIUC. We thank Professor Amit Acharya for comments on the manuscript.

[1] P. Duval, M. F. Ashby, and I. Anderman, J. Phys. Chem. **87**, 4066 (1983).
[2] C. Shearwood and R. W. Whitworth, Philos. Mag. **64**, 289 (1991).
[3] N. A. Fleck, G. M. Muller, M. F. Ashby, and J. W. Hutchinson, Acta Metall. Mater. **42**, 475 (1994).
[4] A. Acharya and A. Roy, J. Mech. Phys. Solids **54**, 1687 (2006).
[5] S. Varadhan, A. J. Beaudoin, and C. Fressengeas, Proc. Sci., SMPRI2005 (2006) 004.
[6] E. Kröner, Erg. Angew. Math **5**, 1 (1958).
[7] T. Mura, Philos. Mag. **8**, 843 (1963).
[8] I. Groma, Phys. Rev. B **56**, 5807 (1997).
[9] A. El-Azab, Phys. Rev. B **61**, 11956 (2000).
[10] R. Sedlacek, J. Kratochvil, and E. Werner, Philos. Mag. **83**, 3735 (2003).
[11] M. Zaiser and T. Hochrainer, Scr. Mater. **54**, 717 (2006).
[12] S. Limkumnerd and J. P. Sethna, Phys. Rev. Lett. **96**, 095503 (2006).
[13] M. Montagnat, P. Duval, P. Bastie, and B. Hamelin, Scr. Mater. **49**, 411 (2003).
[14] M. Montagnat, J. Weiss, J. Chevy, P. Duval, H. Brunjail, P. Bastie, and J. Gil Sevillano, Philos. Mag. **86**, 4259 (2006).
[15] J. F. Nye, Acta Metall. **1**, 153 (1953).
[16] S. Varadhan, A. J. Beaudoin, A. Acharya, and C. Fressengeas, Modelling Simul. Mater. Sci. Eng. **14**, 1245 (2006).
[17] P. J. Armstrong and C. O. Frederick, *A Mathematical Representation of the Multiaxial Bauschinger Effect*, Central Electricity Generating Board Technical Report No. RD/B/N/731, 1966.
[18] F. Louchet, C.R. Physique **5**, 687 (2004).
[19] J. A. Hurtado and J. Weertman, Phys. Status Solidi (a) **149**, 173 (1995).
[20] J. Weertman, Acta Mater. **50**, 673 (2002).